FEBS Letters 586 (2012) 646–652

journal homepage: www.FEBSLetters.org

Review

The cytochrome *f*–plastocyanin complex as a model to study transient interactions between redox proteins

Isabel Cruz-Gallardo, Irene Díaz-Moreno, Antonio Díaz-Quintana, Miguel A. De la Rosa *

Instituto de Bioquímica Vegetal y Fotosíntesis, Centro de Investigaciones Científicas, Isla de la Cartuja (cicCartuja), Universidad de Sevilla-CSIC, Avda. Américo Vespucio 49, Sevilla 41092, Spain

ARTICLE INFO

Article history:
Received 3 July 2011
Revised 8 August 2011
Accepted 24 August 2011
Available online 30 August 2011

Edited by Miguel Teixeira and Ricardo O. Louro

This article is dedicated to the memory of Prof. António V. Xavier

Keywords:
Cytochrome *f*
Electron transfer
Plastocyanin
Transient complex
Photosynthesis

ABSTRACT

Transient complexes, with a lifetime ranging between microseconds and seconds, are essential for biochemical reactions requiring a fast turnover. That is the case of the interactions between proteins engaged in electron transfer reactions, which are involved in relevant physiological processes such as respiration and photosynthesis. In the latter, the copper protein plastocyanin acts as a soluble carrier transferring electrons between the two membrane-embedded complexes cytochrome b_6f and photosystem I. Here we review the combination of experimental efforts in the literature to unveil the functional and structural features of the complex between cytochrome *f* and plastocyanin, which have widely been used as a suitable model for analyzing transient redox interactions.

1. Introduction

Protein–protein interactions are key processes in the proper operation of living cells. Different kinds of interactions can be distinguished on the basis of protein binding affinities. Complexes characterized by low binding affinities occur in transient protein–protein interactions, which display high dissociation equilibrium constants (K_D), within the range of μM–mM, or lifetimes in the order of milliseconds [1,2].

Transient complexes are typical of physiological processes that require a compromise between binding specificity and turnover to run at an appropriate rate [3]. On the basis of a two-step model [4], the formation of a final complex first entails a primary unspecific recognition as an encounter that can be transiently stabilized to yield a productive complex as an outcome.

Electron transfer (ET) reactions are excellent examples of transient complexes. In fact, soluble proteins mediate redox exchange between large membrane complexes in the photosynthetic and respiratory electron transport chains via short-lived interactions. For instance, in oxygenic photosynthesis there is a soluble metalloprotein that shuttles electrons from cytochrome *f* (C*f*), which is a component of the membrane-embedded cytochrome b_6f (Cb_6f) complex, to P700, which is the special chlorophyll pair of Photosystem I (PSI) [5–7]. Either plastocyanin (Pc) or cytochrome c_6 (Cc_6) can play such a role of electron carrier between C*f* and PSI. Higher plants only contain Pc, whereas most cyanobacteria and green algae synthesize either Pc or Cc_6 depending on the relative availability of copper and iron, their respective cofactor metals [8,9].

C*f* is anchored to the thylakoid membrane, within the Cb_6f complex, by a C-terminal transmembrane helix leaving a 28-kDa N-terminal soluble portion exposed to the lumen with a clear two-domain structure. The large domain harbors the heme group, and the small domain possesses a patch of charged residues. C*f* is considered an unusual *c*-type cytochrome because of its β-sheet-based structure, elongated form and particular heme axial

Abbreviations: BD, brownian dynamics; Cb_6f, cytochrome b_6f; Cc_6, cytochrome c_6; C*f*, cytochrome *f*; CSP, chemical-shift perturbations; ET, electron transfer; EXAFS, extended X-ray absorption fine structure; k_2, bimolecular rate constant; K_D, dissociation equilibrium constant; MD, molecular dynamics; NIR, nitrite reductase; NMR, nuclear magnetic resonance; Pc, plastocyanin; PCS, pseudocontact shifts; p*I*, isoelectric point; PRE, paramagnetic relaxation enhancement; PSI, Photosystem I; RMSD, root mean square deviation; WT, wild type; XANES, X-ray absorption near edge structure; XAS, X-ray absorption spectrometry

* Corresponding author. Fax: +34 954460065.
E-mail address: marosa@us.es (M.A. De la Rosa).

0014-5793
doi:10.1016/j.febslet.2011.08.035

coordination with the N-terminus Tyr1 [10,11]. Pc, in its turn, is an 11-kDa cupredoxin with a β-barrel structure formed by eight β-strands and a small α-helix, along with a copper centre coordinated by two histidines, one methionine and one cysteine [12].

The overall structures of both C*f* and Pc are highly conserved from cyanobacteria to higher plants [13–15], but striking differences occur in some of their physical properties. The surface near the heme moiety in C*f* is mainly hydrophobic for all organisms. However, a remarkable basic ridge is found in the small domain for higher plants and green algae turning to acidic in cyanobacteria. On the other hand, Pc relies on two functional sites: a hydrophobic patch surrounding the solvent-accessible histidine copper ligand, or the so-called "site 1", and an electrostatically charged surface area, the so-called "site 2", whose nature varies from one organism to another. Actually, site 2 is mainly acidic in plants and green algae, whereas it ranges from acidic to basic in cyanobacteria. This feature is a key for the dynamics of the complex and is thus herein reviewed.

The C*f*–Pc complex has extensively been studied in the last years as a model to understand the nature of protein–protein interactions in ET chains. The main goal of this article is to briefly review not only our current understanding of the mechanism of ET in transient complexes [16], but also the different techniques used to analyze the structural features of such complexes [17] in an ample set of prokaryotic and eukaryotic organisms.

2. Kinetics within the C*f*–Pc complex

Kinetic analyses provide information about the ET reaction mechanism, namely the limiting step and the nature of the partner interactions. Some years ago, our group proposed three different kinetic mechanisms to analyze the well-related interactions of PSI with Pc and Cc_6 from a wide range of photosynthetic organisms [18–20]. These kinetic models can also be applied to the redox interactions between C*f* and the two soluble carriers Pc and Cc_6 [21–23]. Some of the currently available experimental data for the interaction between C*f* and Pc are summarized in Table 1, where the values for the following constants are presented: bimolecular rate constant for complex formation (k_2), equilibrium constant for association between partners (K_A), and effective electron transfer rate constant (k'_{et}). The interaction between C*f* and Cc_6 cannot be analyzed because of spectral overlapping of the two heme proteins.

Electrostatics determines the kinetics of the C*f*–Pc reaction. In plants, such effect on the ET rate was mainly established by analyzing the interactions of lysine mutants at the basic ridge of turnip C*f* with spinach and pea Pc [21]. Those charged residues at the basic C*f* patch are crucial for the *in vitro* interaction with Pc. Lysines 58, 65 and 187 of C*f* directly interact with acidic residues at site 2 of Pc. The electrostatic attraction between the two partners results in a bell-shaped reaction rate dependence on ionic strength [16] (Fig. 1, *upper panel*). This behavior has been explained by assuming that the complex gets 'locked' in a non-productive electrostatic orientation at low ionic strength. As the ionic strength increases, the rearrangement of both proteins into the complex takes place in order to achieve a well-oriented and productive complex, which corresponds to the maximum of the bell. Further increase in ionic strength leads to complex dissociation [6]. It has recently been proposed that the expression 'locked complex' should be avoided as such a non-productive state at low ionic strength could rather correspond to a set of non-productive orientations slightly different in energy [4].

In vitro kinetic analyses of the interaction between C*f* and Pc in cyanobacteria have mainly been addressed in the mesophilic *Nostoc* [22,24] and thermophilic *Phormidium* [23,25,26] species. The electron transfer rate constant between the two *Nostoc* proteins monotonically decreases with increasing ionic strength (Fig. 1, *middle panel*). The charge mutations at site 2 reduce the ability of Pc to oxidize C*f* [22], whereas the mutations at the hydrophobic patch decrease its reactivity towards the heme protein. It is worth to mention that the charge mutation of Arg93 – a residue of Pc located at the interface between sites 1 and 2 – drastically diminishes the reaction rate, so revealing the crucial role of such amino acid in ET within the complex (Table 1). In contrast, the charge replacements at the small domain of C*f* hardly affect the interaction with Pc [24] (Table 1), thereby suggesting that the specificity in the C*f*–Pc interaction is mostly determined by the cupredoxin. This has been corroborated by NMR studies of the mixed C*f*–Pc complexes between *Nostoc* and *Phormidium* cyanobacterial proteins [27].

The ET rate constant between the wild-type (WT) forms of the two *Phormidium* proteins slightly depends on ionic strength (Fig. 1, *lower panel*), but site-directed mutagenesis of certain charged residues of both proteins revealed a clear influence over the reaction rate (Table 1) [23,25]. Actually, a deeper analysis of the C*f*–Pc complex by continuum electrostatics shows that net coulombic forces between protein charges are slightly repulsive [28]. Assuming a diffusion controlled reaction, the electrostatic forces do influence encounter complex formation. The process also involves specific hydrophobic interactions of aromatic residues in the N-terminal peptide of C*f* [26].

Altogether, the major contribution to k_2 in higher plants and *Nostoc* cyanobacterium is electrostatics, which leads to the encounter between proteins and to the formation of a well-defined

Table 1
Kinetic data for the redox reaction between WT and mutant forms of C*f* and Pc.

C*f*	Pc	k_2 (10^7 M^{-1} s^{-1})	k'_{et} (10^{-3} s^{-1})	K_A (10^3 M^{-1})	References
Turnip WT	Spinach WT	17.6 ± 2.2	~3[a]	–	[21,22]
Turnip K187E	Spinach WT	2.5 ± 0.3	–	–	[21]
Turnip WT	Pea WT	17.5 ± 0.3	–	6.9 ± 0.18	[21]
Turnip K65Q	Pea WT	3.5 ± 0.1	–	0.55 ± 0.38	[21]
Phormidium WT	*Phormidium* WT	4.7[b]	–	~0.3	[23,39]
Phormidium WT	*Phormidium* D44A	6.0[b]	–	–	[23]
Phormidium WT	*Phormidium* R93E	1.0[b]	–	–	[23]
Phormidium D63A	*Phormidium* WT	3.1[b]	–	–	[25]
Nostoc WT	*Nostoc* WT	–	13.4	26 ± 1	[22,27]
Nostoc WT	*Nostoc* D54K	–	25.5	–	[22]
Nostoc WT	*Nostoc* R93E	–	1.8	–	[22]
Nostoc D64A	*Nostoc* WT	–	13.3	–	[24]
Phormidium WT	*Nostoc* WT	–	–	12 ± 1	[27]
Prochlorothrix WT	*Prochlorothrix* WT	~20	–	25 ± 2	[40]

k_2, bimolecular rate constant for complex formation; K_A, equilibrium constant for association between partners; k'_{et}, effective electron transfer rate constant.
[a] French bean Pc was employed.
[b] The overall error of k_2 with all *Phormidium* variants is estimated to be $\leqslant$5%.

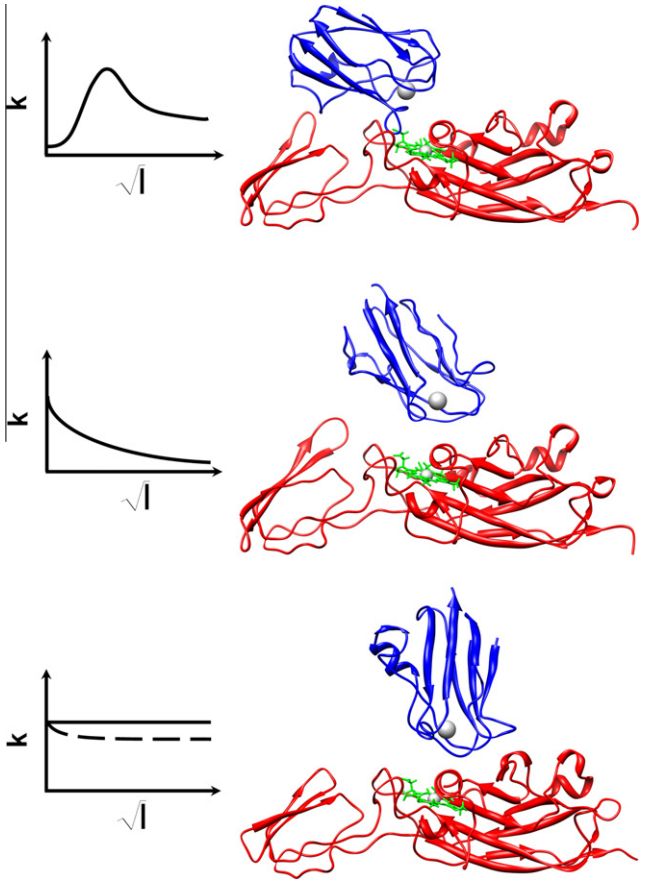

Fig. 1. Comparison of C*f*–Pc complexes from different organisms. *Right*, Superposition of the average structure, with the lowest energy value, calculated from the 10 best NMR structures of each complex. *Left*, profile of the ionic strength dependence of the observed rate constant in each case. *Upper*, poplar [36]; *middle*, *Nostoc* [22,38]; and *lower*, *Phormidium* [25,39]. C*f* and Pc ribbons are in red and blue, respectively. The heme porphyrin ring is depicted in green sticks, whereas the copper and iron atoms are grey spheres.

functional complex. The opposite is valid for the thermophilic *Phormidium* cyanobacterium, in which non-polar interactions play the main role because of the small net contribution of electrostatics [23,26,28]. Nevertheless, the hydrophobic interactions are essential for ET in all complexes, since the reorganization of water molecules at the interface should impair the charge transfer process. In fact, the exclusion of water molecules yields a productive complex within which the ET takes place. Intriguingly, the reaction rates reach similar values under physiological salt concentration and temperature ($k_2 \sim 10^8$ M^{-1} s^{-1}) despite the apparent differences among organisms [23].

In vivo approaches are quite scarce. In the alga *Chlamydomonas reinhardtii* [29,30], neutralization of C*f* basic ridge has a negligible effect on the rate of protein re-oxidation, suggesting that electrostatic interactions within the C*f*–Pc complex are not so relevant *in vivo* in this organism. Experimental conditions mimicking viscosity, macromolecular crowding and temperature have also been explored, but no relevant conclusions can be reached [31].

3. Defining the relative orientation between C*f* and Pc

The structure of the C*f*–Pc complex, as well as that of the C*f*–Cc_6 one, has been analyzed by nuclear magnetic resonance (NMR) spectroscopy [17,32] by using the chemical and pseudo-contact shifts (PCS) experienced by the Pc signals as restraints for rigid-body docking calculations. Diamagnetic, chemical-shift perturbations (CSP) are caused by changes in the chemical environment suffered by the atoms located at the binding interface. Structural restrains derived from CSP do not provide precise geometrical information about angles and distances between the two partners. However, measuring PCS renders geometrical restraints that may be sufficient to define the relative orientation of both proteins. PCS restraints are provided by the intrinsic paramagnetic probe of C*f*, which supplies the oxidized iron atom (Fe^{3+}) from the heme phorphyrin ring. PCS depend on the axial and rhombic components of the magnetic susceptibility tensor and the angles that the vector joining the heme Fe atom of C*f* to the target amide proton in Pc forms with them. Moreover, PCS are inversely proportional to the cubed distance between any particular nucleus of Pc and the paramagnetic center. Structure elucidation of the C*f*–Pc complex for different organisms shown in this section fits well with the orientation of C*f* within the Cb_6*f* complex as determined by X-ray crystallography [11,33].

Some similar structural features, like interface areas of ca. 600–850 Å^2 per protein, are shared by the C*f*–Pc complexes from prokaryotic and eukaryotic organisms. All the cases studied show that Cu-ligand His87 in Pc is close to iron-coordinating Tyr1 in C*f*, thereby providing an efficient electron transfer pathway [34]. However, remarkable differences are found not only when comparing the structures of plant and cyanobacterial complexes, but also when the comparisons are made between complexes from cyanobacteria (Fig. 1).

Plant heterologous complexes between C*f* from turnip and Pc from several other sources like spinach, parsley or poplar have been solved [35–37]. Their overall structures show a binding mode named *side-on* (Fig. 1, *upper panel*) in which the hydrophobic patches of the two proteins keep in close contact with each other and the complementary charged regions are juxtaposed. In other words, both Pc sites 1 and 2 are involved in the binding interface. The Fe–Cu distance varies from 10.9 Å in spinach to 13.9 Å in poplar and 13.0 Å in parsley. Actually, poplar and parsley Pc are slightly tilted with regard to the position of spinach Pc [36]. Within the poplar C*f*–Pc complex, the approach of the side-chain of His87 from Pc to the heme ring at C*f* is restricted by the loop containing this copper ligand. In contrast, the parsley C*f*–Pc model shows a rotation of Pc, with respect to the spinach, in a direction opposite to that in poplar complex [37].

The cyanobacterial complexes have been analyzed using both Pc and C*f* from the same source. The structure of the C*f*–Pc complex from *Nostoc* [38] shows a relative orientation that resembles the plant *side-on* fashion, but with the charges reversed. Actually, the positive charged residues at site 2 of *Nostoc* Pc – which indeed are determinant in the isoelectric point (p*I*) of 8.4 for the whole protein – are keeping salt bridges with negative residues at the hinge and small domain of C*f*. However, the p*I* of plant Pc is ca. 4.0 and its negatively charged site 2 interacts with the positive charged residues of C*f*. The hydrophobic interactions involving the two metal centers of both proteins are also present (Fig. 1, *middle panel*). In contrast, Pc in the *Phormidium* complex is oriented in a *head-on* manner relative to C*f*, with only site 1 (hydrophobic patch) making contact to C*f* (Fig. 1, *lower panel*). In *Phormidium*, C*f* lacks the typical basic ridge, whereas Pc has fewer charged residues at site 2 [39] than Pc from plants and shows a dipole moment aligned with the main molecule axis. This results in the attraction of the copper site towards C*f* and repulsion of site 2. The resulting net coulombic term between the two proteins is repulsive, but is mostly compensated by solvent polarization phenomena to yield a small ionic strength effect [28]. The *Phormidium* complex shows a highly dynamic nature that could explain the lower precision of the solved structure – with an RMSD of 3.7 Å – compared with other C*f*–Pc models. It could also be explained by differences in

the dynamic behavior of the complexes, a fact that is especially significant in those organisms that inhabit niches at high temperatures.

Crossed complexes between proteins from *Nostoc* and *Phormidium* revealed that it must be a low net electrostatic contribution in the latter complex [27], in agreement with results on ET kinetics. Although early NMR data [39] suggested the absence of electrostatic interactions, several transient conformations involving electrostatics could remain invisible by NMR, at least in the absence of paramagnetic relaxation enhancement measurements (PRE). Therefore, only the long-life conformation into the complex is detectable. In addition, studies of such mixed complexes show that the differences in interactions are mainly attributable to the surface properties of Pc [27]. The NMR analyses (PCS measurements) show that the C*f*–Pc complex from *Prochlorothrix hollandica*, unlike the *Nostoc* C*f*–Pc complex, exhibits a *side-on* orientation, in which Pc site 2 is not interacting with the small domain of C*f*, thereby suggesting a dynamic nature that resembles the *Phormidium* complex [40].

An overall view of structural features for the well-defined oriented C*f*–Pc complexes postulates a predominant *side-on* conformation highly dependent on electrostatics. As the electrostatic contribution becomes lower, the orientation of Pc relative to C*f* shifts from *side-on* to *head-on.* All these observations are also in agreement with the ET proposed kinetic mechanisms.

4. Metal cofactors within the C*f*–Pc complex

Although there are a lot of experimental data on the interaction between the two redox partners, the information on the effect of binding on the metal cofactors and their properties is rather scarce. In fact, the redox potential of Pc decreases in 30 mV upon binding to C*f* [41]. Noteworthy, the way on how metal sites can adapt to changes in the protein matrix and modulate the ET reaction highly contributes to understand the transient complexes involved in this kind of processes.

The cyanobacterial *Nostoc* C*f*–Pc complex has been analyzed by X-ray absorption spectroscopy (XAS). Both Fe and Cu K-edge XAS measurements of free and bound redox proteins have been studied in solution, using either the oxidized or reduced species [42,43].

In C*f*, the Fe atom of the heme group is axially coordinated by two nitrogen atoms belonging to Tyr1 (N) and His26 ($N_{\epsilon 2}$). Such atypical coordination geometry involves the N-terminal tyrosine, which also takes part in hydrophobic interactions with Pc, according to the structural elucidations of this transient complex [38]. XAS measurements reveal that the Fe coordination geometry remains unaltered upon binding to Pc. Getting a deeper insight into the data, a slight distortion of the metal (Fe^{2+}) center geometry seems to happen when reduced C*f* binds to reduced Pc. The resulting geometry is closer to that of oxidized C*f*, either free or bound to oxidized Pc. Because of the smaller size of Fe^{3+} compared to Fe^{2+}, the first fits better than the second into the heme group as Fe^{2+} is slightly out of the plane [44]. However, Fe^{2+} could be driven back to the ring upon complex formation. Iron-N-terminus nitrogen bond in C*f* is strong enough to prevent distortions over the coordination geometry of the metal center, so facilitating a stable binding site to Pc and enhancing ET.

The copper atom in Pc is coordinated by two nitrogen atoms from His39 and His92, as well as by two sulphur atoms from Cys89 and Met97. All of them are well-conserved residues placed at a protein loop that is at the interface with C*f* [35,38,39]. Cu–K edge XAS shows a remarkable distortion in the trigonal pyramidal geometry of the copper coordination sphere upon binding to C*f*, regardless of its redox state (Fig. 2, *upper* and *middle panel*). The main evidence for such a distortion is the contribution of the S_δ atom from Met97 to the extended X-ray absorption fine structure (EXAFS) wave, indicating that the mobility of this side-chain is substantially restrained upon binding of Pc to C*f*. Actually, the resulting tetrahedral structure of the copper center within the C*f*–Pc complex exhibits a shorter Cu–Sδ(Met97) distance with respect

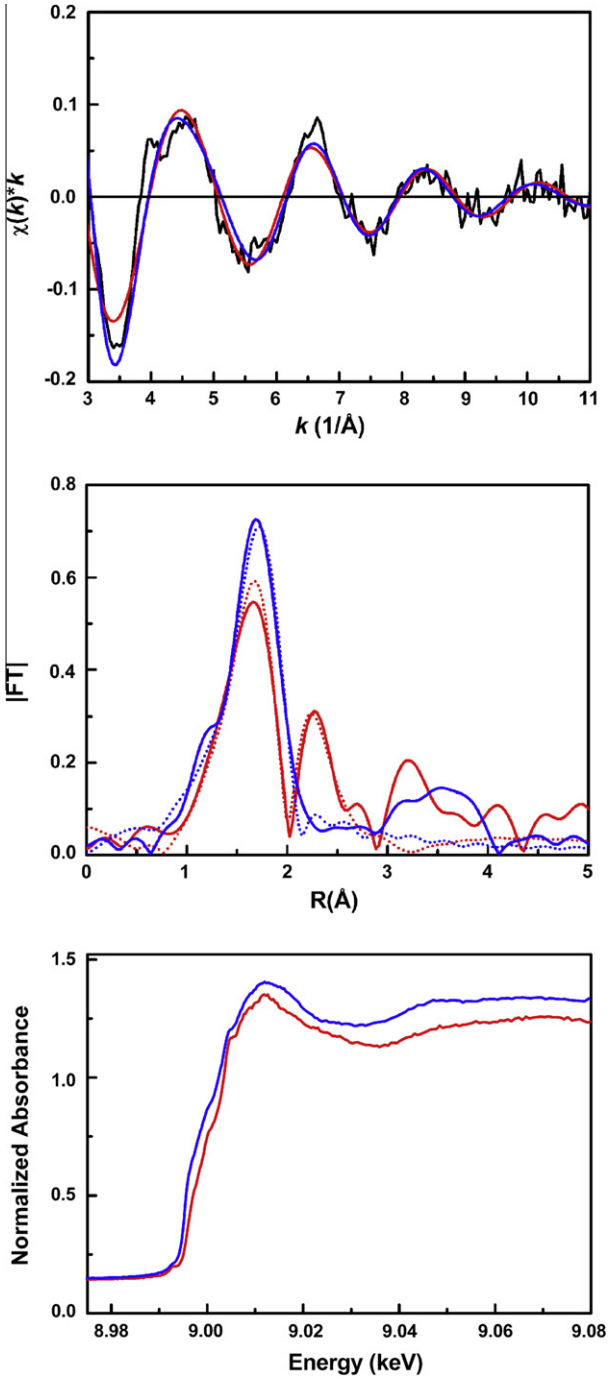

Fig. 2. Distortion of the copper geometry of Pc upon C*f* binding in *Phormidium*. *Upper*, EXAFS spectra at the Cu K-edge of oxidized Pc upon binding to oxidized C*f* (black) and fitting in the k space either considering that the contribution of S_δ(Met97) is negligible (red, χ^2: 16.97) or taking it into account (blue, χ^2: 11.3). *Middle*, Fourier Transform modules of free Pc (blue) and Pc-bound to C*f* (red), both in the reduced state. The best fits for the data are depicted in dotted lines following the same color-code. The contribution of the S_δ(Met97) atom is considered for the fit in R space. *Lower*, XANES region of the Cu K-edge XAS spectra for free Pc (blue) and Pc-bound to C*f*, both in the oxidized state (red).

to the crystallographic structure of free Pc [45]. Noteworthy, the Cu–Sδ(Met97) distance of C*f*–bound Pc by EXAFS resembles that of the crystal structure of oxidized nitrite reductase (NIR) [46], which belongs to the so-called "perturbed" copper centers. In addition, the electronic density around the copper atom increases when Pc binds to C*f* in their oxidized states, according to the data from the X-ray absorption near edge structure (XANES) region (Fig. 2, *lower panel*). In fact, the redox potential of Pc becomes more negative upon binding to C*f* [41]. As a result, the driving force for ET between both metalloproteins is significantly decreased by the C*f*–Pc interaction. In addition, the observed geometrical changes in the first coordination sphere of copper within the C*f*–Pc complex modulate the electron coupling along the different ET pathways and hence the redox reaction.

5. Theoretical approaches

The resulting data from analyzing the weak C*f*–Pc complex by means of theoretical methods add useful information to our current knowledge of transient interactions.

The C*f*–Pc complexes of a wide range of organisms, from cyanobacteria to plants, have been studied by Brownian Dynamics (BD) simulations using crystal or NMR structures. The role of electrostatic interactions in higher plant and algal complexes has been confirmed by BD simulations that are in good agreement with the k_2 values for ET reactions previously reported [21,23,25]. The complex between turnip C*f* and spinach Pc [47] and that between C*f* and Pc from the green alga *Chlamydomonas reinhardtii* [48] have both been studied by performing systematic mutations of charged residues at the protein interfaces. These data support the model of an electrostatically driven encounter complex as a previous step of a final productive complex wherein efficient ET occurs. BD analyses with *Phormidium* C*f* and Pc from different sources [49] show considerable variations in electrostatic forces, a finding that highlights the key role of a few charged residues close to His92 (His87 in plants and algae) for the complex interface. However, the computational studies show that Pc is highly mobile in all these complexes, opposite to its behavior in plant complexes. Still, hydrophobic interactions remain highly significant in all organisms.

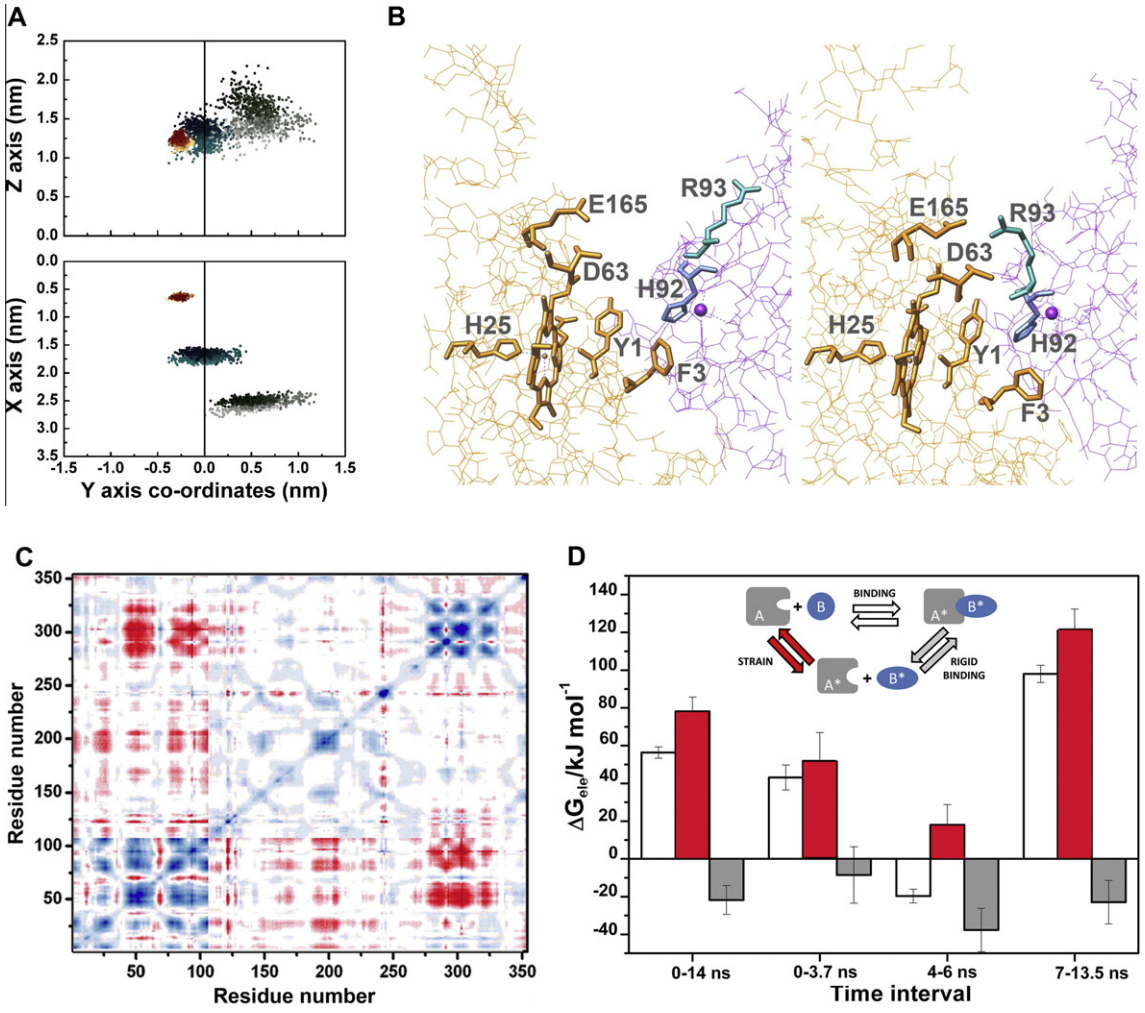

Fig. 3. Molecular dynamics of the *Phormidium* C*f*–Pc complex. (A) Drift of Pc around C*f* along the MD trajectory in Ref. [28]. The dihedral first angle projections of the trajectories of iron from C*f* (brown dots), copper (blue dots) and center of mass of Pc (grey dots) are represented with respect to the main axes and mass center of the large domain of C*f*. (B) Interaction of the copper site and Arg93 in Pc with negative residues of C*f* upon approaching of the two partners. Pc and copper center are in purple, and C*f* in gold. The side chains of charged residues and the heme porphyrin ring are depicted in sticks following the same color-pattern. (C) Coordinate covariance matrix of a trajectory corresponding to the C*f*–Pc complex obtained after aligning main chain atoms of the large domain of C*f*. Residues 1–105 correspond to Pc, and 106–354 to C*f* Positive values are shown in blue, whereas negative are in red. (D) Analysis of continuum electrostatics averaged along different time intervals of a MD computation of the C*f*–Pc complex. The insert summarizes the thermodynamic cycle used in the computation of the different terms in which $\Delta G_{ele\text{-}bind}$ stands for the sum of free energies that account for distorting the free monomers to get the conformation they adopt in the complex, $\Delta G_{ele\text{-}strain}$, and their subsequent rigid-body association, $\Delta G_{ele\text{-}rigid}$. $\Delta G_{ele\text{-}bind}$ is represented by white bars; $\Delta G_{ele\text{-}strain}$ by red-filled bars; $\Delta G_{ele\text{-}rigid}$ bars are colored in grey.

BD analyses are quite sensitive to small changes in conformation of the proteins that are being modeled. For instance, the C*f*–Pc complex with spinach Pc adopted two different conformations when using distinct structural data sources [50]. On the basis of such finding, it was suggested that Pc may assume distinct conformations in solution so as to yield a productive ET complex.

BD and other docking approaches treat proteins as rigid bodies [40], whereas Molecular Dynamics (MD) calculations provide additional information about internal protein motions. Despite all the kinetic, structural and theoretical studies performed on the *Phormidium* C*f*–Pc complex, there is certain controversy regarding NMR and functional data. Hence, MD simulations combined to continuum electrostatic calculations on this particular interaction [28] try to harmonize the two sets of data. The MD trajectories reveal that Pc tilts towards the small domain of C*f* approaching site 2 to the heme protein (Fig. 3A). This involves the interaction of the positive charges of the copper site and Arg93 with the negatively charged residues at the loop of C*f* surrounding the heme group (Fig. 3B). Thus, the relative orientation of Pc respect to C*f* in the *Phormidium* complex can be redefined as a *tilted head-on* conformation (see Fig. 1, *lower panel*). However, the repulsive forces make both proteins swing in an opposite but concerted manner within the transient C*f*–Pc complex, as inferred from the negative covariance between motions of Pc and those of the small domain of C*f* (Fig. 3C). Interestingly, the conformation of C*f* is strained upon binding of its partner and relaxes upon release. Although there are no direct contacts between Pc and the small domain of C*f*, continuum electrostatic calculations indicate that the long-range electrostatic interactions between them are responsible for straining the conformation of the partners (Fig. 3D). The thermodynamic cycle shown in Fig. 3D reveals that $\Delta G_{\text{ele-bind}}$ can be split in two terms if any one of the partners changes within the complex. The first term is the "strain energy" ($\Delta G_{\text{ele-strain}}$), which accounts for the cost of structural changes needed for docking; the second one is the "rigid binding" ($\Delta G_{\text{ele-rigid}}$) component, which represents the binding energy of the strained partners. Fig. 3D also shows that the time intervals corresponding to the two major ensembles of conformations (from 0 to 3.7 ns, and from 7 to 13 ns) are characterized by a positive $\Delta G_{\text{ele-strain}}$ term and by large strain energy values ($\Delta G_{\text{ele-bind}}$). However, $\Delta G_{\text{ele-bind}}$ becomes negative, with a concomitant drop in $\Delta G_{\text{ele-strain}}$, in the time interval from 4 to 6 ns corresponding to the transition between these two major populations. An explanation for this binding energy decrease comes from the reaction field term that accounts for solvent polarization phenomena. In addition, the electrostatic strain may play a key role in breaking the complex off after the attraction between the copper surroundings and C*f* is weakened upon charge transfer.

6. Conclusion and outlook

A multidisciplinary effort has been made in the last years to understand the behavior of transient ET complexes and, in particular, of the short-lived C*f*–Pc complex from different organisms. In most cases, the functional and structural approaches coincide in postulating the relevance of long-range electrostatic interactions *in vitro*. The existence of an encounter complex may indeed play an important role in the C*f*–Pc complexes, a finding that should be further explored in detail. Some controversy still exists over experimental data interpretation in the cyanobacterial model system from *Phormidium*, but theoretical simulations are providing valuable information to conciliate them. Actually, recent modeling developments could help to widen the scope of this subject. The bottleneck is to unveil the relevance of these data *in vivo*. Specifically, the role played by electrostatics on the ET process inside crowded cells needs further research.

Acknowledgements

The authors wish to thank the Spanish Ministry of Science and Innovation (BFU2009-07190) and the Andalusian Government (BIO198 and P08-CVI-3876) for financial support.

References

[1] Perkins, J.R., Diboun, I., Dessailly, B.H., Lees, J.C. and Orengo, C. (2010) Transient protein–protein interactions: structural, functional, and network properties. Structure 18, 1233–1243.
[2] Janin, J. (2000) Kinetics and thermodynamics of protein–protein interactions in: Protein–protein recognition (Kleanthous, C., Ed.), pp. 1–32, Oxford University Press, Oxford.
[3] Bashir, Q., Scanu, S. and Ubbink, M. (2011) Dynamics in electron transfer protein complexes. FEBS J. 278, 1391–1400.
[4] Ubbink, M. (2009) The courtship of proteins: Understanding the encounter complex. FEBS Lett. 583, 1060–1066.
[5] Allen, J.F. (2004) Cytochrome b_6f: structure for signalling and vectorial metabolism. Trends Plant Sci. 9, 130–137.
[6] Hervás, M., Navarro, J.A. and De la Rosa, M.A. (2003) Electron transfer between membrane complexes and soluble proteins in photosynthesis. Acc. Chem. Res. 36, 798–805.
[7] Sun, J., Xu, W., Navarro, J.A., Hervás, M., De la Rosa, M.A. and Chitnis, P.R. (1999) Oxidizing side of the cyanobacterial photosystem I: evidence for interaction between the electron donor proteins and a lumenal surface helix of the PsaB subunit. J. Biol. Chem. 274, 19048–19054.
[8] De la Rosa, M.A., Navarro, J.A., Hervás, M., De la Cerda, B., Molina-Heredia, F.P., Balme, A., Murdoch, P.S., Díaz-Moreno, I., Durán, R.V. and Hervás, M. (2002) An evolutionary analysis of the reaction mechanisms of photosystem I reduction by cytochrome c_6 and plastocyanin. Bioelectrochemistry 55, 41–45.
[9] Durán, R., Hervás, M., De la Rosa, M.A. and Navarro, J.A. (2004) The efficient functioning of photosynthesis and respiration in *Synechocystis* sp. PCC 6803 strictly requires the presence of either cytochrome c6 or plastocyanin. J. Biol. Chem. 279, 7229–7233.
[10] Martinez, S.E., Huang, D., Szczepaniak, A., Cramer, W.A. and Smith, J.L. (1994) Crystal structure of chloroplast cytochrome f reveals a novel cytochrome fold and unexpected haem ligation. Structure 2, 95–105.
[11] Stroebel, D., Choquet, Y., Popot, J.L. and Picot, D. (2003) An atypical haem in the cytochrome b_6f complex. Nature 426, 413–418.
[12] Coleman, P.M., Freeman, H.C., Guss, J.M., Murata, M., Norris, V.A., Ramshaw, J.A.M. and Venkatappa, M.P. (1978) X-ray crystal structure analysis of plastocyanin at 2.7 Å resolution. Nature 272, 319–324.
[13] Carrel, C.J., Schlarb, B.G., Bendall, D.S., Howe, C.J., Cramer, W.A. and Smith, J.L. (1999) Structure of the soluble domain of cytochrome f from cyanobacterium *Phormidium laminosum*. Biochemistry 38, 9590–9599.
[14] Bond, C.S., Bendall, D.S., Freeman, H.C., Guss, J.M., Howe, C.J., Wagner, M.J. and Wilce, M.C.J. (1999) The structure of plastocyanin from the cyanobacterium *Phormidium laminosum*. Acta Cryst. D55, 414–421.
[15] Chi, Y.I., Huang, L.S., Zhang, Z., Fernández-Velasco, J.G. and Berry, E.A. (2000) X-ray structure of a truncated form of cytochrome f from *Chlamydomonas reindhardtii*. Biochemistry 39, 7689–7701.
[16] Hope, A.B. (2000) Electron transfers amongst cytochrome f, plastocyanin and photosystem I: kinetics and mechanisms. Biochim. Biophys. Acta 1456, 5–26.
[17] Ubbink, M. (2004) Complexes of photosynthetic redox proteins studied by NMR. Photosynth. Res. 81, 277–287.
[18] Hervás, M., Navarro, J.A., Díaz, A., Bottin, H. and De la Rosa, M.A. (1995) Laser-flash kinetic analysis of the fast electron transfer from plastocyanin and cytochrome c_6 to photosystem I. Experimental evidence on the evolution of the reaction mechanism. Biochemistry 34, 11321–11326.
[19] Hervás, M., Navarro, J.A., Díaz, A. and De la Rosa, M.A. (1996) A comparative thermodynamic analysis by laser-flash absorption spectroscopy of photosystem I reduction by plastocyanin and cytochrome c6 in *Anabaena* PCC 7119, *Synechocystis* PCC 6803, and spinach. Biochemistry 35, 2693–2698.
[20] De la Cerda, B., Navarro, J.A., Hervás, M. and De la Rosa, M.A. (1997) Changes in the reaction mechanism of electron transfer from plastocyanin to photosystem I in the cyanobacterium *Synechocystis* sp. PCC 6803 as induced by site-directed mutagenesis of the copper protein. Biochemistry 36, 10125–10130.
[21] Gong, X.S., Wen, J.Q., Fisher, N.E., Young, S., Howe, C.J., Bendall, D.S. and Gray, J.C. (2000) The role of individual lysine residues in the basic patch on turnip cytochrome f for electrostatic interactions with plastocyanin *in vitro*. Eur. J. Biochem. 267, 3461–3468.
[22] Albarrán, C., Navarro, J.A., Molina-Heredia, F.P., Murdoch, P.S., De la Rosa, M.A. and Hervás, M. (2005) Laser flash-induced kinetic analysis of cytochrome f oxidation by wild-type and mutant plastocyanin from the cyanobacterium *Nostoc* sp. PCC 7119. Biochemistry 44, 11601–11607.
[23] Schlarb-Ridley, B.G., Bendall, D.S. and Howe, C.J. (2002) Role of electrostatics in the interaction between cytochrome f and plastocyanin of the cyanobacterium *Phormidium laminosum*. Biochemistry 41, 3279–3285.
[24] Albarrán, C., Navarro, J.A., De la Rosa, M.A. and Hervás, M. (2007) The specificity in the interaction between cytochrome f and plastocyanin from the cyanobacterium *Nostoc* sp. PCC 7119 is mainly determined by the copper protein. Biochemistry 46, 997–1003.

[25] Hart, S.E., Schlarb-Ridley, B.G., Delon, C., Bendall, D.S. and Howe, C.J. (2003) Role of charges on cytochrome f from the cyanobacterium *Phormidium laminosum* in its interaction with plastocyanin. Biochemistry 42, 4829–4836.
[26] Schlarb-Ridley, B.G., Bendall, D.S. and Howe, C.J. (2003) Relation between interface properties and kinetics of electron transfer in the interaction of cytochrome f and plastocyanin from plants and the cyanobacterium *Phormidium laminosum*. Biochemistry 42, 4057–4063.
[27] Díaz-Moreno, I., Díaz-Quintana, A., De la Rosa, M.A., Crowley, P.B. and Ubbink, M. (2005) Different modes of interaction in cyanobacterial complexes of plastocyanin and cytochrome. Biochemistry 44, 3176–3183.
[28] Díaz-Moreno, I., Muñoz- López, F.J., Frutos-Beltrán, E., De la Rosa, M.A. and Díaz-Quintana, A. (2009) Electrostatic strain and concerted motions in the transient complex between plastocyanin and cytochrome f from the cyanobacterium *Phormidium laminosum*. Bioelectrochemistry 77, 43–52.
[29] Soriano, G.M., Ponamarev, M.V., Piskorowski, R.A. and Cramer, W.A. (1998) Identification of the basic residues of cytochrome f responsible for electrostatic docking interactions with plastocyanin *in vivo*: relevance to the electron transfer *in vivo*. Biochemistry 37, 15120–15128.
[30] Soriano, G.M., Ponamarev, M.V., Tae, G.S. and Cramer, W.A. (1996) Effect of interdomain basic region of cytochrome f on its redox reactions *in vivo*. Biochemistry 35, 14590–14598.
[31] Schlarb-Ridley, B.G., Mi, H., Teale, W.D., Meyer, V.S., Howe, C.J. and Bendall, D.S. (2005) Implications of the effects of viscosity, macromolecular crowding, and temperature for the transient interactions between cytochrome f and plastocyanin from the cyanobacterium *Phormidium laminosum*. Biochemistry 44, 6232–6238.
[32] Crowley, P.B., Díaz-Quintana, A., Molina-Heredia, F.P., Nieto, P., Sutter, M., Haehnel, W., De la Rosa, M.A. and Ubbink, M. (2002) The interactions of cyanobacterial cytochrome c_6 and cytochrome f, characterized by NMR. J. Biol. Chem. 277, 48685–48689.
[33] Kurisu, G., Zhang, H., Smith, J.L. and Cramer, W.A. (2003) Structure of the cytochrome b6f complex of oxygenic photosynthesis: tuning the cavity. Science 302, 1009–1014.
[34] Díaz-Quintana, A., Hervás, M., Navarro, J.A. and De la Rosa, M.A. (2008) Plastocyanin and cytochrome c6: the soluble electron carriers between the cytochrome b6f complex and photosystem I in: Structure of photosynthetic proteins (Fromme, P., Ed.), pp. 181–200, Wiley-VCH, Weinheim, Germany.
[35] Ubbink, M., Ejdeback, M., Karlsson, B.G. and Bendall, D.S. (1998) The structure of the complex of plastocyanin and cytochrome f, determined by paramagnetic NMR and restrained rigid-body molecular dynamics. Structure 6, 323–335.
[36] Lange, C., Cornvik, T., Díaz-Moreno, I. and Ubbink, M. (2005) The transient complex of poplar plastocyanin with cytochrome f: effects of ionic strength and pH. Biochim. Biophys. Acta 1707, 179–188.
[37] Crowley, P.B., Hunter, D.M., Sato, K., McFarlane, W. and Dennison, C. (2004) The parsley plastocyanin-turnip cytochrome f complex: a structurally distorted but kinetically functional acidic patch. Biochem. J. 378, 45–51.
[38] Díaz-Moreno, I., Díaz-Quintana, A., De la Rosa, M.A. and Ubbink, M. (2005) Structure of the complex between plastocyanin and cytochrome f from the cyanobacterium *Nostoc* sp. PCC 7119 as determined by paramagnetic NMR. J. Biol. Chem. 280, 18908–18915.
[39] Crowley, P.B., Otting, G., Schlarb-Ridley, B.G., Canters, G.W. and Ubbink, M. (2001) Hydrophobic interactions in a cyanobacterial plastocyanin-cytochrome f complex. J. Am. Chem. Soc. 123, 10444–10453.
[40] Hulsker, R., Baranova, M.V., Bullerjahn, G.S. and Ubbink, M. (2008) Dynamics in the transient complex of plastocyanin and cytochrome f from *Prochlorothrix hollandica*. J. Am. Chem. Soc. 130, 1985–1991.
[41] Malkin, R., Knaff, D.B. and Bearden, A.J. (1973) The oxidation–reduction potential of membrane-bound chloroplast plastocyanin and cytochrome f. Biochim. Biophys. Acta 305, 675–678.
[42] Díaz-Moreno, I., Díaz-Moreno, S., Subías, G., De la Rosa, M.A. and Díaz-Quintana, A. (2006) The atypical iron-coordination geometry of cytochrome f remains unchanged upon binding to plastocyanin, as inferred by XAS. Photosynth. Res. 90, 23–28.
[43] Díaz-Moreno, I., Díaz-Quintana, A., Díaz-Moreno, S., Subías, G. and De la Rosa, M.A. (2006) Transient binding of plastocyanin to its physiological redox partners modifies the copper site geometry. FEBS Lett. 580, 6187–6194.
[44] Schnackenberg, J., Than, M.E., Mann, K., Wiegand, G., Huber, R. and Reuter, W. (1999) Aminoacid sequence, crystallization and structure determination of reduced and oxidized cytochrome c_6 from the green alga *Scenedesmus obliquus*. J. Mol. Biol. 290, 1019–1030.
[45] Schmidt, L., Christensen, H.E.M. and Harris, P. (2006) Structure of plastocyanin from the cyanobacterium *Anabaena variabilis*. Acta Cryst. D 62, 1022–1029.
[46] Adman, E.T., Godden, J.W. and Turley, S. (1995) The structure of copper-nitrite reductase from *Achromobacter cycloclastes* at five pH values, with NO_2 bound and with type II copper depleted. J. Biol. Chem. 270, 27458–27474.
[47] De Rienzo, F., Gabdoulline, R.R., Menziani, M.C., De Benedetti, P.G. and Wade, R.C. (2001) Electrostatic analysis and Brownian dynamics simulation of the association of plastocyanin and cytochrome f. Biophys. J. 81, 3090–3104.
[48] Haddadian, E.J. and Gross, E.L. (2005) Brownian dynamics study of cytochrome f interactions with cytochrome c_6 and plastocyanin in *Chlamydomonas reinhardtii*: plastocyanin and cytochrome c_6 mutants. Biophys. J. 88, 2823–2839.
[49] Gross, E.L. and Rosenberg, A. (2006) A Brownian dynamics study of the interaction of *Phormidium* cytochrome f with various cyanobacterial plastocyanins. Biophys. J. 90, 366–380.
[50] Gross, E.L. (2007) A Brownian dynamics computational study of the interaction of spinach plastocyanin with turnip cytochrome f: the importance of plastocyanin conformational changes. Photosynth. Res. 94, 411–422.